Optical and Structural Properties of Rutile Nanoparticles Prepared Via Ball Milling

Abstract

This study centered on determining the optical characteristics of Rutile nanoparticles and synthesizing them using a ball milling process. A top-down approach was utilized to obtain nanoparticles from the bulk materials utilizing high intensity ball milling technique. The crystalline size of the nanoparticle was ascertained using the Debye-Scherer formula.TheEnergy Band gap, optical conductivity, extinction coefficient, transmittance, and refractive index were among the optical characteristics that were identified. The average crystalline size obtained, was 87.440 nm. The computed dislocation density varied between$(0.109 \times 10^{-3} to\ 0.0359 \times 10^{-3}) nm^{-2}$. As the wavelength range shifted from the ultraviolet to the visible and near-infrared regions, the absorbance value was observed to decrease simultaneously.The refractive index of the particle showed a uniform result from 1eV to 4eV but sharply increased at 4.1eV and also dropped sharply at 4.3eV and then maintained a uniform outcome as the photon energy increased. The transmittance value was also observed to gradually increase from the ultraviolet region, to the visible region, hence reaching 99.9%in the near-infrared region. Furthermore, the band energy gap was obtained to be 3.88 eV. The unique properties of the Rutile nanoparticles revealed potential uses in photovoltaic and optoelectronic systems.

Keywords: Rutile; nanoparticle; crystalline size; optical properties; band energy gap.

1.0 Introduction

In today's world, materials play a vital role in our daily lives and exploring the unique characteristics of the materials at the nano scales has become increasingly important. These nanoparticles are usually products of nanotechnology whose particles are less than 100nm (Onu et al.2023). However, the properties of the nanoparticles, present specific and controllable properties that are different from those they represent on the macroscopic scale thus enabling unique applications (Yetter et al. 2009; Srivastava et al. 2009; Shalini et al. 2012). The change in properties is due to two main effects: (i) surface effects or size reduction effect which implies that when a particle size is reduced, a greater proportion of atoms are found at the surface (ii) quantum confinement-modification in electronic structure (Srivastava et al. 2009; Gupta and Gupta 2005; Aline et al. 2010).

It has been observed that the ratio between the number of surface atoms and the number of massive atoms increases significantly with particle size reduction so that the surface atoms have

less coordination in relation to massive atoms. This resulted in nanostructured materials exhibiting significantly different physical, chemical, optical, mechanical, electrical and also magnetic properties (Chaturvedi et al. 2013; Yetter et al. 2009). Due to these characteristics, nanoscale materials present great potential for applications in several technological areas such as Nano electronics and computer technology, medicine, aeronautics and space exploration, biotechnology and agriculture (Srivastava et al. 2009).These nano-composites have copious importance in semiconducting industries, optoelectronic industries and photocatalytic industries (Madkhali et al. 2022; Onu et al. 2024). Futhermore, nanoparticles have been reported to have applications in environmental filed for water treatment, gas sensors, solar photocatalysisetc (Onu et al. 2023).

The extensive utilization of nanoparticles is predicated on their distinct features, which typically differ from those of bulk materials. Most nanoparticles possess a substantial energy gap, exceptional ultraviolet emission capabilities, and a satisfactory binding energy (Rong et al 2018; Onu et al 2023). Moreover, they possess considerable stability and the capability to alter the electrical conductivity of gases, along with an inherent aptitude to absorb ultraviolet radiation (Liu et al. 2011; Madkhali et al. 2022; Onu et al. 2023).

There are two primary ways for nanoparticle preparation: the top-down method (deconstruction) and the bottom-up method (construction) (Satoshi and Nick 2013; Onu et al. 2023). The top-down approach entails applying an external force to a much reduced bulk solid material, resulting in its fragmentation into smaller nanoparticles while the bottom-up approach involves changing and transforming liquids or gaseous atoms into comparatively bigger nanoparticles by atomic transformation or molecular condensation.

Therefore, the top-down approach was used, which entails milling or grinding comparatively substantial material into nanoparticles. Since the milling technique is known to be suitable for creating widely dispersed nanoparticles that prevent the condensation of freshly formed nanoparticles (Satoshi and Nick 2013; Onu et al. 2023).

Through the mechanical process of ball milling, a greatly reduced substance is subjected to the kinetic energy of moving balls, which breaks down the chemical bonds and produces nanoparticles (Tan et al. 2013; Carmen et al. 2019; Onu et al. 2023). This will produce

nanoparticles with novel surfaces and characteristics (Joy et al. 2022). This high energy milling has been proven to be a highly effective method for processing bulk materials. This technique offers several benefits, including: Efficient particle size reduction, simplified processing, cost-effectiveness, broad material applicability and scalability to large quantities (Zhang et al. 2014).

Investigations into the effects of various ball milling parameters on bulk samples properties have demonstrated the versatility and potential of this technique. Ball milling has attracted considerable attention and is an effective physical mechanical milling synthesis method owing to the relatively low installation cost, the large number of particles can be easily obtained by solely grinding bulk materials in a milling vessel.

Rutile is an accessory natural occurring mineral in a variety of metamorphic and igneous rocks it also occurs as a detrital mineral in clastic sediments. Although the main formula of rutile is TiO_2, there are commonly several possible substitutions for titanium, for example, Al, V, Cr, Fe, Zr, Nb, Sn, Sb, Hf, Ta,W and U (Graham and Morris, 1973; Hassan, 1994; Murad et al., 1995; Smith and Perseil, 1997; Rice et al. 1998; Zack et al. 2002; Bromiley and Hilairet, 2005; Scott, 2005; Carruzzo et al., 2006).Variations in the geochemical composition are host rock specific and allow the rutile source to be traced and the chemical and physical properties during rutile formation to be characterized.

Titanium dioxide (TiO_2) is among the most useful materials for many applications due to its nontoxicity, low cost, physical and chemical stability, availability and optical properties (Wang et al. 2016). Titanium dioxide (TiO_2) exists as three different phases; anatase, rutile and brookite (Zhang et al. 2014) and its band gaps ranges from (3.0 – 3.2 eV). Hence the aim of this research is to prepare nanoparticles from Rutile bulk materials and determine its structural and optical properties.

2.0 Materials and Methods

2.1 Sourcing and Preparation of the samples

The Rutile was sourced from Taraba state in Nigeria, the Rutile ore were initially crushed manually into tiny pebbles because of their comparatively considerable bulkiness. This is to prepare it for the experiment with the ball mill.

2.2 Preparation of the Nanoparticle through Bia milling Technique

The ball milling experiment was carried out in a planetary ball milling machine located in Faculty of Engineering, Department of mechanical Engineering, NnamdiAzikiwe University Awka. It has vials steel balls inside about 10.0mm diameter to prepare the fine nanoparticles. The Rutile was introduced through the milling lid. The milling was done in ambient atmosphere.

A constant ball-to-powder weight ratio of 10:1 (wt/wt) was maintained during the operation. The ball milling was performed in a horizontal operation technique at 25 Hz. The milled materials were used directly with no added milling media. The ball milling was for a total of 10 hours with some time intervals which helped in avoiding undesirable rapid increase in temperature inside the milling vial. After the ball milling experiment, the milled nanoparticles were taken out for specific particle size sieving.

2.3Particle size sieving of the prepared nanoparticles

A mechanical sieve shaker (model: OCIASION 2022) was used to sieve the nanoparticles.The milled nanoparticles were introduced through the top sieve tray. When the power is switched on, the vibration of the shaker makes the finer nanoparticles placed at the top sieve tray to pass through the sieve size and down to the next lower tray. Again, the finer particles that can pass through that sieve size will pass through it down to the next sieve tray. The process continues until the finest nanoparticle sizes have reached the last sieve tray. Then the nanoparticles were collected for characterization.

3.0 Characterization

3.1 X-ray Diffraction technique

It is also known as x-ray diffractometer. XRD is a popular technique used for the analysis of the structural properties and the identification of minerals in solid state and nanoparticle sizes. As

seen in figure 1, abruker D 5005 power X-ray diffraction with Ni-filtered, C_u,K_x-radiation was used to record diffraction spectra, prior to the measurement, each sample was prepared using a standard method for powdered sample preparation. The sample was dried in the over at 100^{o}C. About 1g of each sample was grinded to fine powder and homogenized as much as possible, then loaded into the poly-methyl mete-acrylate sample holder. The powder was gently pressed into the cavity using a glass slide, while the glass was gently lifted off to reveal the sample surface. Each diffraction spectrum recorded with condition 2θ angle of between 5^o and 50^o, Cu-target, 35Kv, 35mA and scan speed of 0.3 degree/0.02 second. Typically, the data was expressed in the plot between intensity of diffraction peaks and 2θangle. The positions of diffraction peaks were compared with a reference data base and the identifications of compounds calculated.

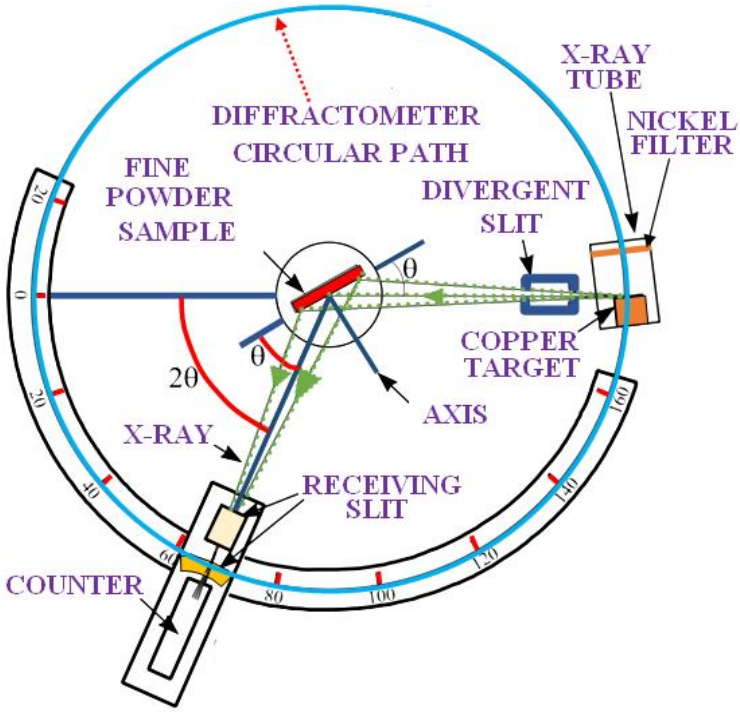

Figure 1: Schematic diagram of X-ray diffraction technique.

3.2Optical Analysis (UV Spectroscopy)

UV-Vis spectroscopy is an analytical technique that measures the amount of discrete wavelengths of UV or visible light that are absorbed by or transmitted through a sample in comparison to a reference, control or blank sample as shown in figure 2. However, one gram of Rutile was dispersed in ethanol. The sample was passed through the instruments which have two lamps, tungsten or halogen lamp commonly used for visible light, whilst a deuterium lamp is the

common source of UV light.As two different light sources are needed to scan both the UV and visible wavelengths, the light source in the instrument was switch on during measurement. This switchover typically occurred during the scan between 300 and 350 nm where the light emission is similar from both light sources so that the transition can be made more smoothly.

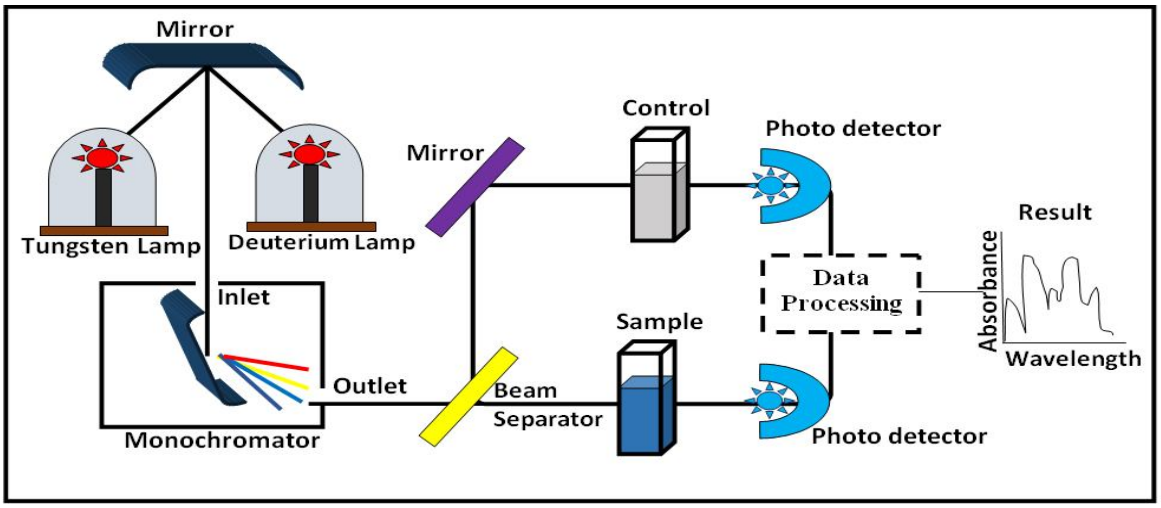

Figure 2. Schematic diagram of UV-vis spectrophotometer.

4.0 Result and Discussion

4.1 X-ray Diffraction and Crystal Analysis

The structural and lattice properties of the Rutile particle were evaluated from the x-ray diffraction (XRD) analysis. The analysis revealed that the full width at half maximum ranged from0.090 – 0.163 nm. While the nanoparticle distance spacing ranged from1.682 - 3.222 Å

The nanoparticle crystalline size was obtained using Debye-Scherer formula given in equation 1 (Ashraf et al. 2015; Sutapa et al. 2018; Onu et al. 2023)

$$D = \frac{0.9\lambda}{\beta \cos\theta} \qquad (1)$$

Where, K representthe Scherrer constant usually 0.9,β is full width at half maximum (FWHM), λ is the x-ray wavelength (0.15406 nm) and is Bragg's diffraction angle.

Dislocation density of nanoparticles was calculated by using equation 2 (Sutapa et al. 2018; Onu et al. 2023).

$$D_d = \frac{1}{D^2} \quad (2)$$

Where D_d is the dislocation density and D is the crystalline size

The results obtained are tabulated in Table 1 below. The crystalline size ranged from52.776nm to 95.529 nm with an average crystalline size of87.740 nm. The full width at half maximum showed an indirect relationship with crystalline size.

This dislocation density calculated ranged from$(0.109 \times 10^{-3} to\ 0.0359 \times 10^{-3}) nm^{-2}$. The dislocation density defines the number of dislocation lines per unit volume of crystals. Since dislocation density obtained from the analysis is small, the nanoparticles prepared have a high degree of crystallinity (Sutapa et al. 2018; Onu et al. 2023).

Table 1. Crystal properties of the Rutile

2θ, °	**Lattice spacing d, (Å)**	**FWHM, ° (β)**	**Miller indices (hkl)**	**Crystalline size (nm)**	**Dislocation density $(nm)^{-2}$**
27.66	3.222	0.162	111	52.776	0.000359
32.696	2.737	0.163	112	54.410	0.000337
36.316	2.472	0.090	123	95.529	0.000109
54.525	1.682	0.112	246	83.613	0.000143

The XRD diffraction pattern shown in Figure 3 reveal a distinct peaks were observed at 2theta angles of 27.66,32.69,36.31,and 54.52 corresponding to miller indices of 111, 112, 123, and 246 respectively on the crystallographic planes (Mbonu, 2015; Falak, 2010). The peaks might have resulted due to contaminants in the sample, some XRD peaks are left out without indexing. The effect of impurities on the crystal structure has a significant role in the change of the physical properties (Saleem *et. al.,* 2016). The XRD spectrum demonstrated the nanoparticles polycrystalline composition.

4.2Absorption spectra of Rutile particles

The absorption spectra of the Rutile particles dispersed in ethanol is depicted in figure 4. The Rutile particles showed relatively high absorbance within the range of 40.9% to 65.8% at the

ultraviolet region. However, at the ultraviolet region a constant decrease in the absorbance was observed within 45.4% to 63.6%. At the visible region it decreases further to 35.5% showing low absorbance. Similar results were also gotten by previous studies as revealed in Table 2. The absorbance was near zero at the near-infrared regions indicating that the Rutile particles are non-absorbing at the near-infrared regions.

Table 2: Optical results of previous studies in comparative with the present study.

Research Title	Number of sample studies	Method of synthesis	Absorbance result	Transmittance result	Band gap	Reference
Structural and Optical properties of TiO_2 thin films prepared by spin coating	4	Sol gel	A low absorbance value was seen in the visible range for the number of layers	All samples revealed a high transmittance in the visible range with an average transmittance value ranging from 80 to 92 % with the number of layers	3.54 and 3.75eV	Sta et al. (2014)
Optical and Electrical Properties Dependence on Thickness of Screen-Printed TiO_2 Thin Films	4	Electrode deposition	A low absorbance was observed in all the films within the visible range	The samples showed high transmittance in the visible region within the range of 68% to 78%	3.5, 3.6, 3.7 and 3.8 eV	Domtau et al. (2016)
Investigation of Optical Properties of TiO_2 Nano Powder	1	Chemical precipitation	Very low absorbance was observed from the spectrum in the visible region	The mean transmittance of the semiconductor metal oxide TiO_2 in the visible region was calculated as 89.72 %	3.219 eV	Fehmi et al. (2020)
Structure and optical properties of Titanium Dioxide thin film with mixed Fluorine and Indium doping for solar cell components	5	Sol gel	All the samples showed low absorbance in the visible region	The results showed that the transmittance value was very low in the ultraviolet region but increased in the wavelength range of 350–700 nm (visible light region) given as 73.76, 73.01, 72.78, 71.01 and 69.55%.	3.83; 3.80; 3.79; 3.79; and 3.75 eV	Doyan et al. (2022)

Optical and Structural Properties of Rutile Nanoparticles Prepared Via Ball Milling	1	Ball milling	A low absorbance value was seen in the visible range for the number of layers	The sample revealed a high transmittance in the visible range with an average transmittance value of 92.8%	3.88 eV	Present Study (2025)

4.3 Transmittance of Rutile

The transmittance was obtained from the absorbance as the exponent of the negative value of the absorbance. Figures 5 the transmittance spectra of the Rutile particles dispersed in ethanol.The transmittance was observed to be zero at the wavelength of 200 – 300nm within the ultraviolet region before it began to increase as it approaches visible region, it increases up to 92.8% in the visible region and increases further to 99.9% in the near-infrared region. Similar results were also gotten by previous studies as revealed in Table 2.The plot revealed a Low transmittance in the ultraviolet region while relatively high transmittance was observed in the near-infrared and the visible regions of the spectra, this was also reported by (Ozobialu et al.2022; Onu et al. 2023).This shows that Rutile particles have good optical transmission in the visible and near-infrared spectrum. These results also showed that the Rutile particles can be utilized in optoelectronic and photovoltaic devices.

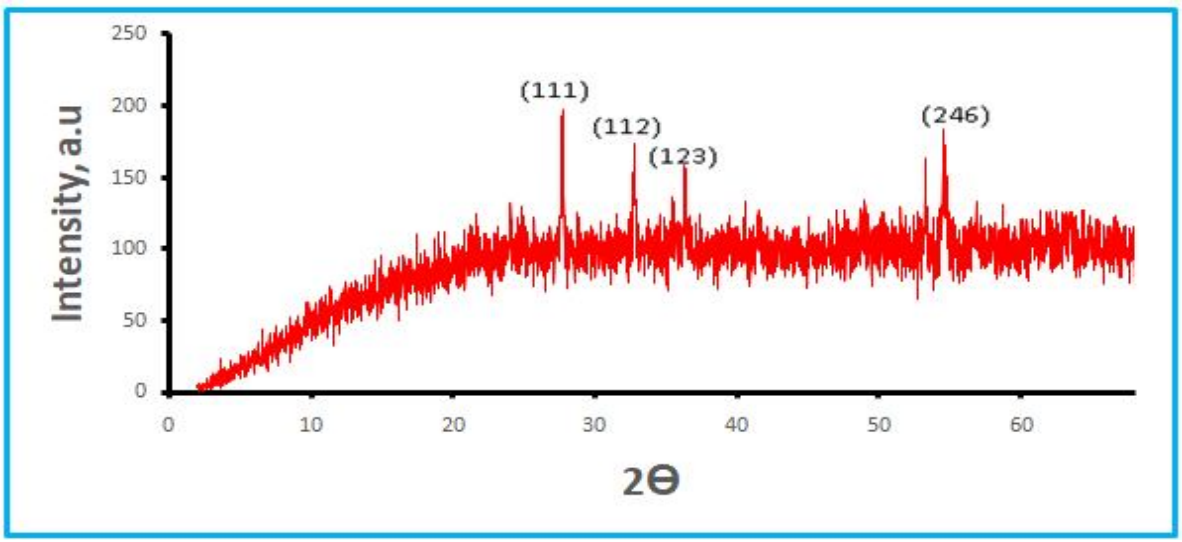

Figure 3: X-ray diffraction pattern

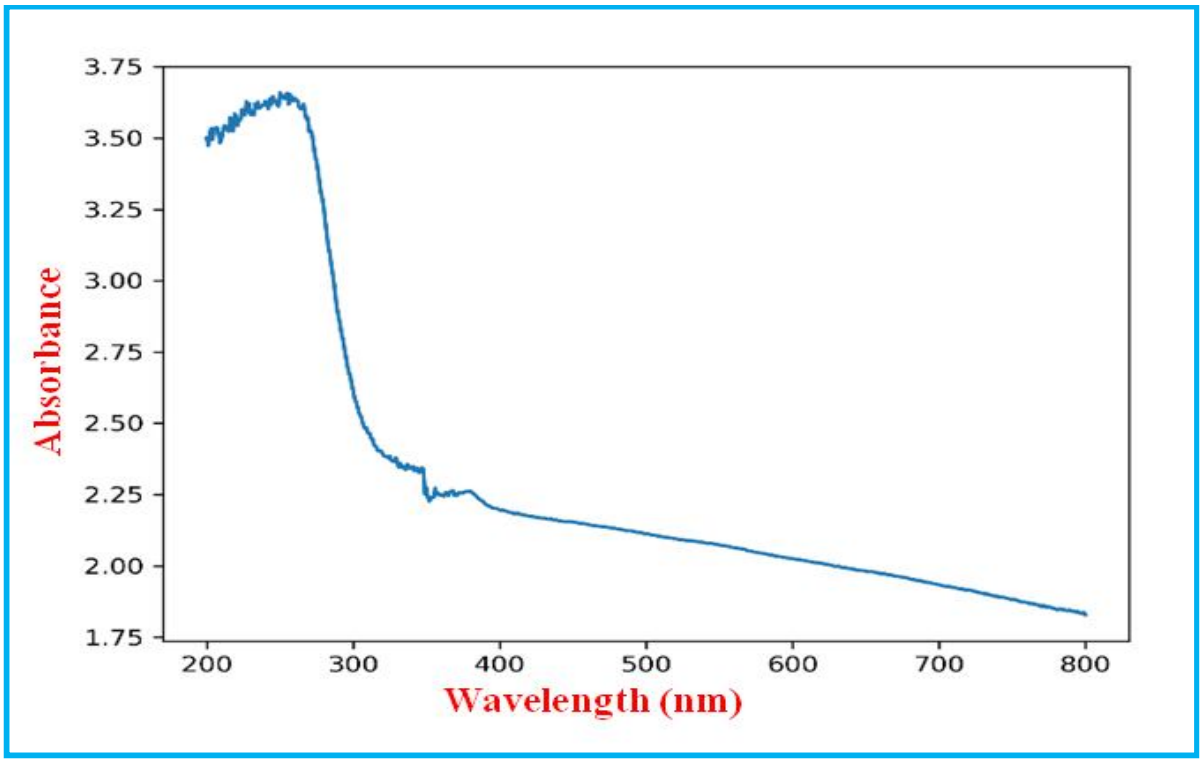

Figure 4: Plot of absorbance against wavelength

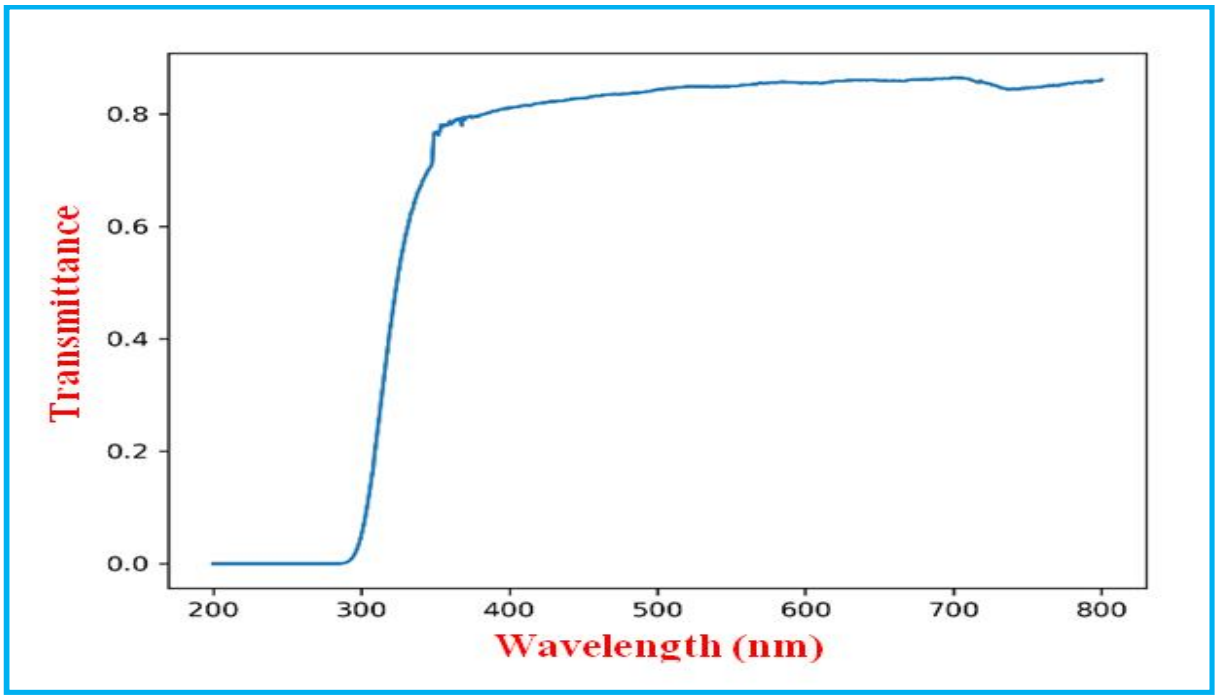

Figure 5: Plot of Transmittance against wavelength

4.4 Reflectance of Rutile

The plot of the reflectance of the Rutile particles as a function of wavelength is shown in figure 6. The plot revealed that the ethanol dispersed Rutile particles initially increases irregularly from 66.6% to 70.6% before it then decreases sharply to 34.6% in the ultraviolet region and it was also observed to increase irregularly just before the visible region. However, in the visible region it also decreases sharply and approach zero in the near-infrared region of the spectrum. This have been reported that low reflectance are always observed at visible region (Okafor et al. 2022) Hence, the poor reflectivity over the whole spectrum indicates it can be utilized in the window layer of a solar cell (Wanjala et al 2016; Simon et al. 2022; Onu et al. 2023).

4.5 Refractive index of Rutile

The refractive index was determined from the reflectance values. The plot of the refractive index of the Rutile particles as a function of photon energy can be seen in figures 7. Therefractive index of ethanol dispersed particle showed a uniform result from 1eV to 4eV and sharply increased at 4.1eV. Hence it was seen to sharply decrease at 4.3 eV and then maintained a uniform outcome as the photon energy increased. This suggests that the refractive index of Rutile particles can be adjusted to influence their matrix properties at the molecular level (Hiroshi et al. 2016). The refractive index is contingent upon wavelength and influences the interaction between nanoparticles and light in diverse applications (Edwin et al. 2014). Also, the refractive index in the semiconductor is a measure of its transparency to incident spectral radiation (Onu et al. 2024).

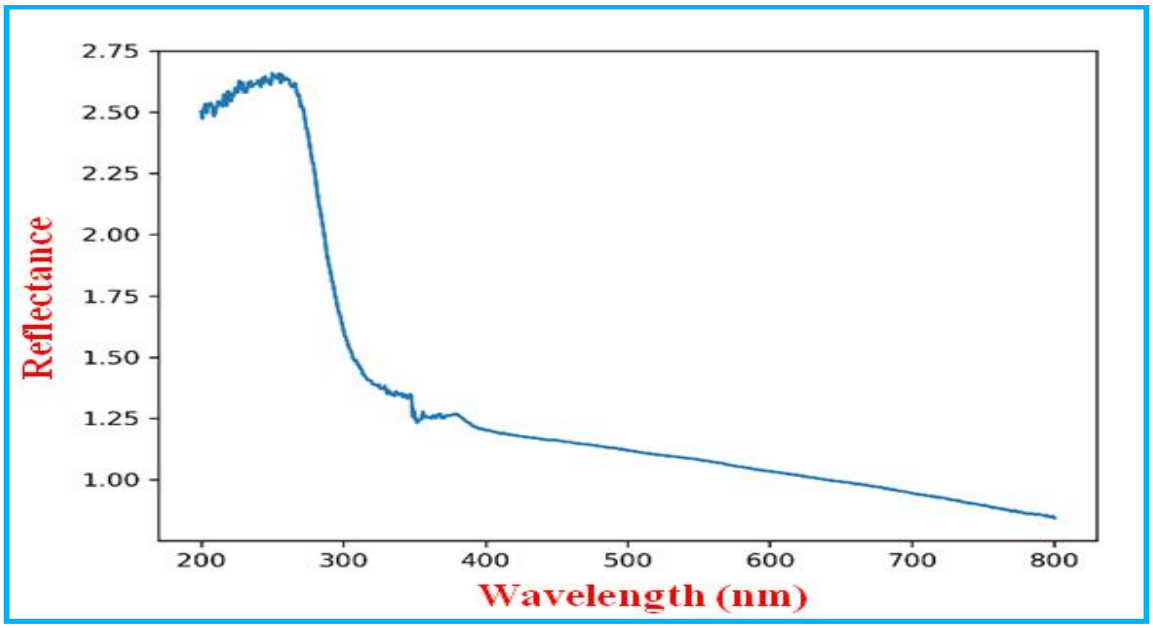

Figure 6: Plot of Reflectance against wavelength

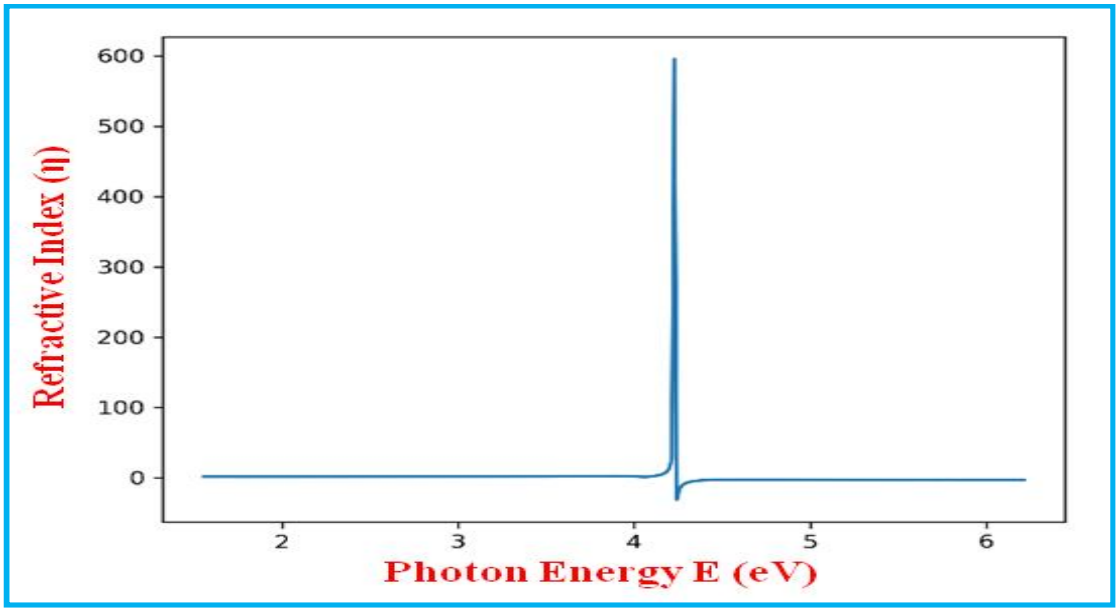

Figure 7: Plot of Reflective index against Photon energy

4.6Absorption coefficient of Rutile

Absorption coefficient is a direct function of absorbance and wavelength of the particles. The variation of absorption coefficient of the Rutile particles with wavelengths was shown in figure 8. It was observed from the plot that the absorption coefficient of the Rutile particles dispersed in ethanol decreases as wavelength increases. However, the absorption coefficient of Rutile was

almost constant at near-infrared region with further increase in the wavelength. This high absorption coefficient of the Rutile particles at the ultraviolet region and visible region indicates the ability of Rutile films to absorb light in these regions.

4.7 Extinction coefficient of Rutile

The extinction coefficient of the Rutile particles was determined from the absorption coefficient and the wavelength. The plot of the extinction coefficients is a function of absorption coefficient and wavelength. This is presented in figures 9.The extinction coefficient of the Rutile particles dispersed in ethanol initially increases irregularly and then decreased sharply in the ultraviolet region, it then increased irregularly before decreasing progressively in the visible region and the reduction continued towards the near-infrared region.According to Krohnke (2001); Onu et al. (2023) a relatively high extinction coefficient indicates the capacity to naturally release absorbed energy as heat rather than harmful radiation.

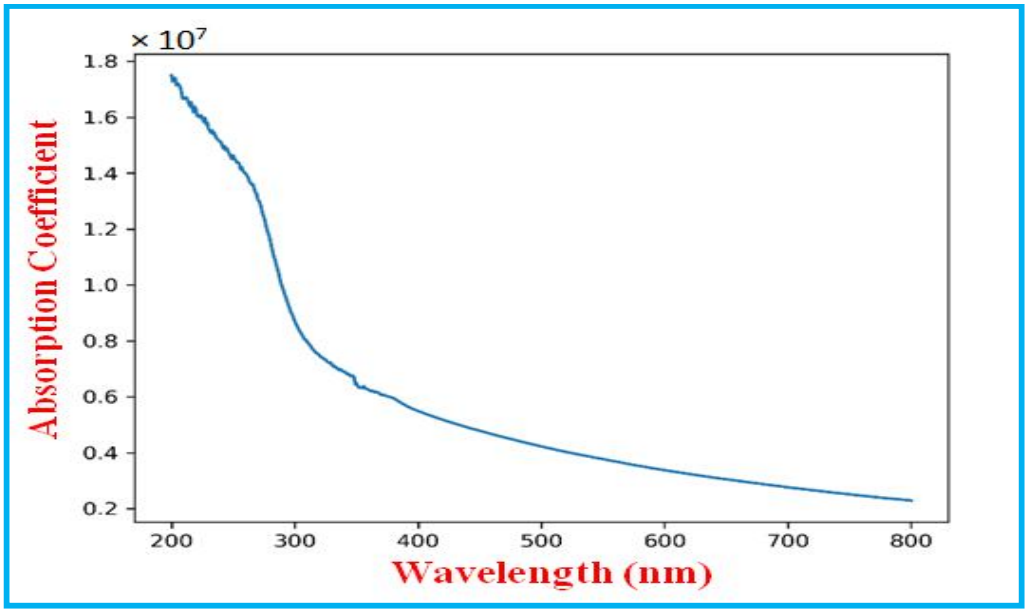

Figure 8: Plot of Absorption coefficient against wavelength

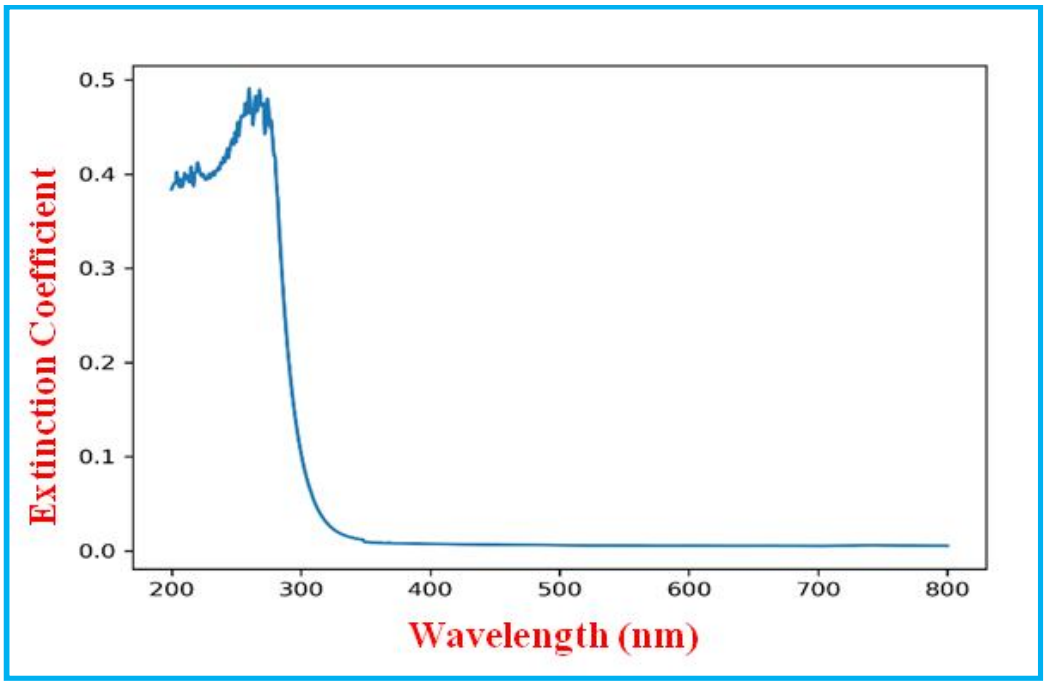

Figure 9: Plot of Extinction Coefficient against wavelength

4.8 Real Dielectric constant of Rutile

The real part dielectric constant was calculated by deducting the square of the extinction coefficient from the square of the refractive index (Noor et al. 2019; Onu et al. 2023). The variation of the real part dielectric constant with photon energy was presented in figures10 for the ethanol dispersed Rutile particle. However, the dielectric constant remained at zero throughout the whole spectrum except for the sudden rise and fall observed at 2eV.

4.9 Imaginary dielectric constant of Rutile

A variation of the imaginary dielectric constant of the Rutile particles with photon energy was presented in figures 11. According to Noor et al. (2019); Onu et al 2023 the imaginary dielectric constant can be evaluated as twice the product of extinction coefficient and the refractive index of the particle. Hence imaginary dielectric constant is a function of the extinction coefficient and the refractive index. The results showed that for the ethanol dispersed Rutile particles the imaginary dielectric constant was stable as photon energy increases aside the abrupt increase and decrease observed at 2eV of the photon energy.

4.10 Optical conductivity of Rutile

The plots of the optical conductivity against the photon energy are shown in figures 12 According to Al-Hammadi and Sadiq (2023), optical conductivity is given as a function of absorption coefficient and the refractive index of the material. The results showed that for the ethanol dispersed Rutile particles the optical conductivity was stable as photon energy increases aside the abrupt increase and decrease observed at 2eV of the photon energy. The optical conductivity shows the rate of absorption of incident photons (Choudhary et al. 2022; Onu et al. 2023).The correlation between current density and a material's exposure to various light wavelengths in an electric field is governed by optical conductivity, which is crucial for determining the atomic structure of the particles (Onu et al. 2023). Additionally, optical conductivity plays a decisive role in shaping the spectra of specific nanoparticles. Furthermore, optical conductivity is essential in determining the spectra of particular nanoparticles.

4.11 Band energy gap of Rutile

The band energy gap is the smallest amount of energy required to excite an electron to a state where it may conduct in the conduction band (Onu et al. 2023).According to Jothibas et al. (2017), the optical band gap with direct transition can be calculated from equation 3

$$\propto \quad v = A(\quad v - Eg)^n \qquad (3)$$

Where v is the photon energy, A is a constant that depends on the transition probability, $\propto$ is the absorption coefficient, Eg is the optical band gap and n is a number that characterizes the transition process. The band energy gap is major parameter used in the design of optoelectronic instruments (AL. Hammadi and Sadiq 2013). The direct band gap was obtained by extrapolating the linear Tauc plots of (αhv^2against v).This implies that the optical band gap of the Rutile nanoparticles sample was extracted from thecurve shown in figure 13. So that the bang gap of Rutile dispersed in ethanol was obtained to be 3.88eV

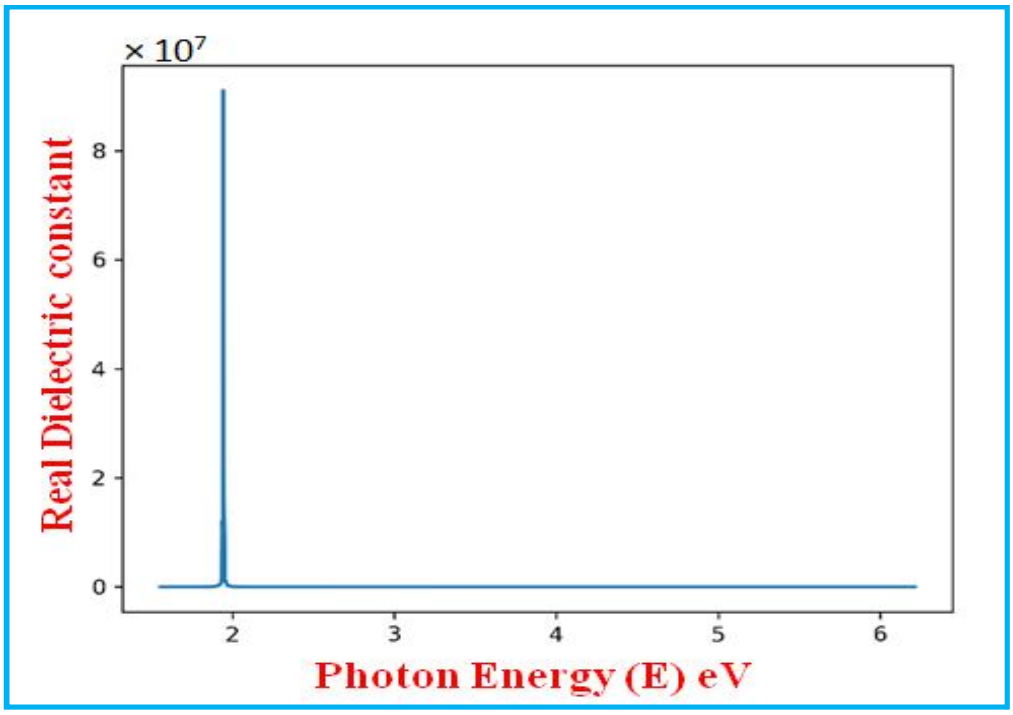

Figure 10: Plot of real dielectric constant against photon energy

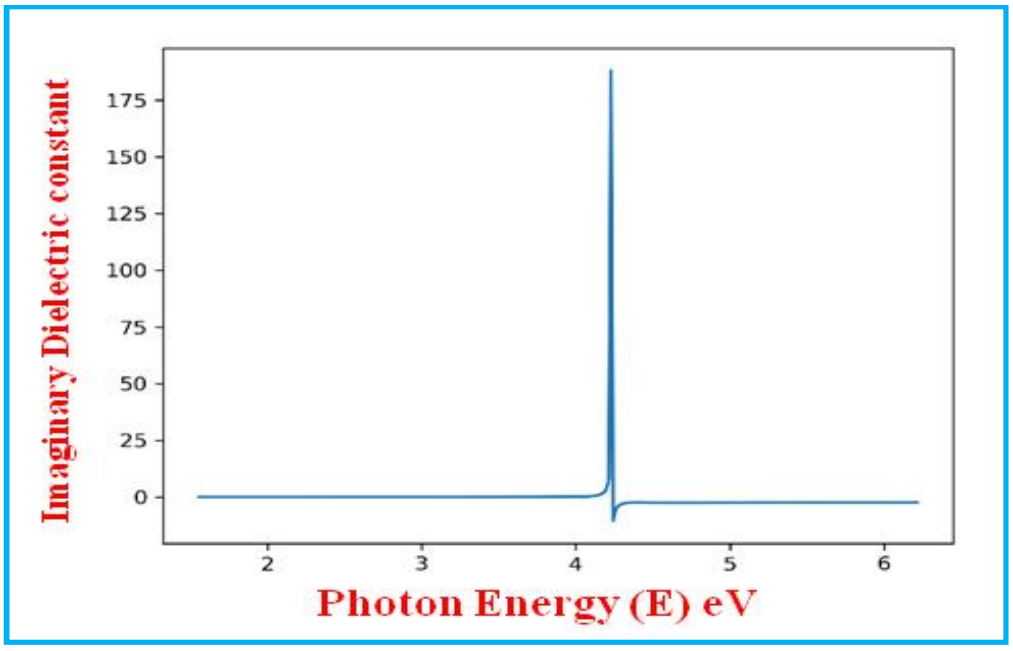

Figure 11: Plot of imaginary dielectric constant against photon energy

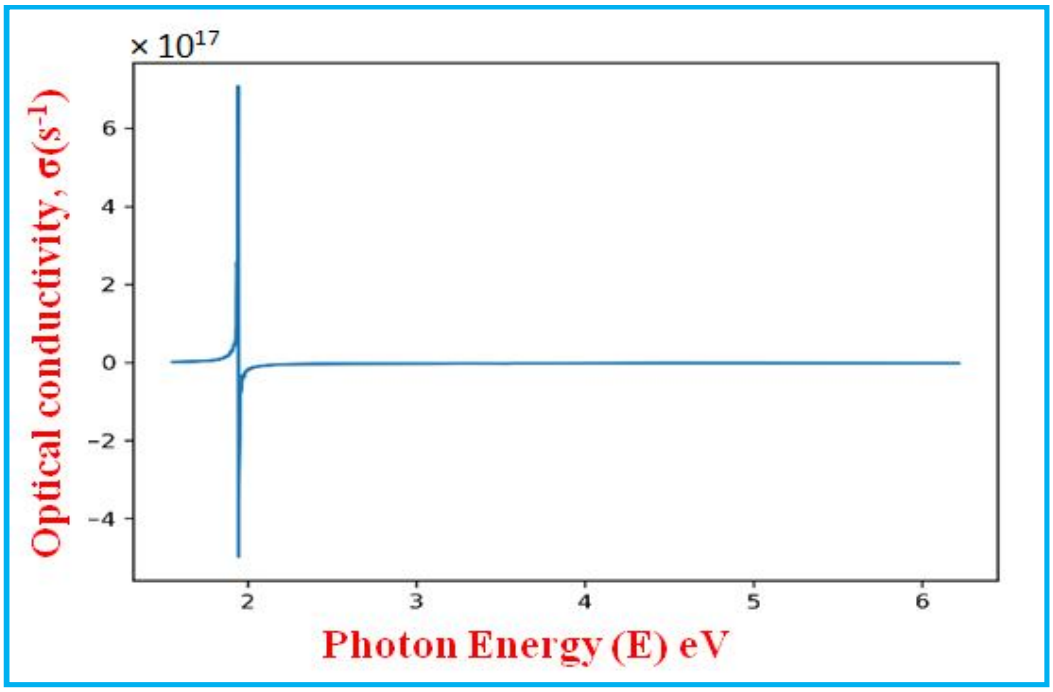

Figure12. Plot of optical conductivity against photon energy

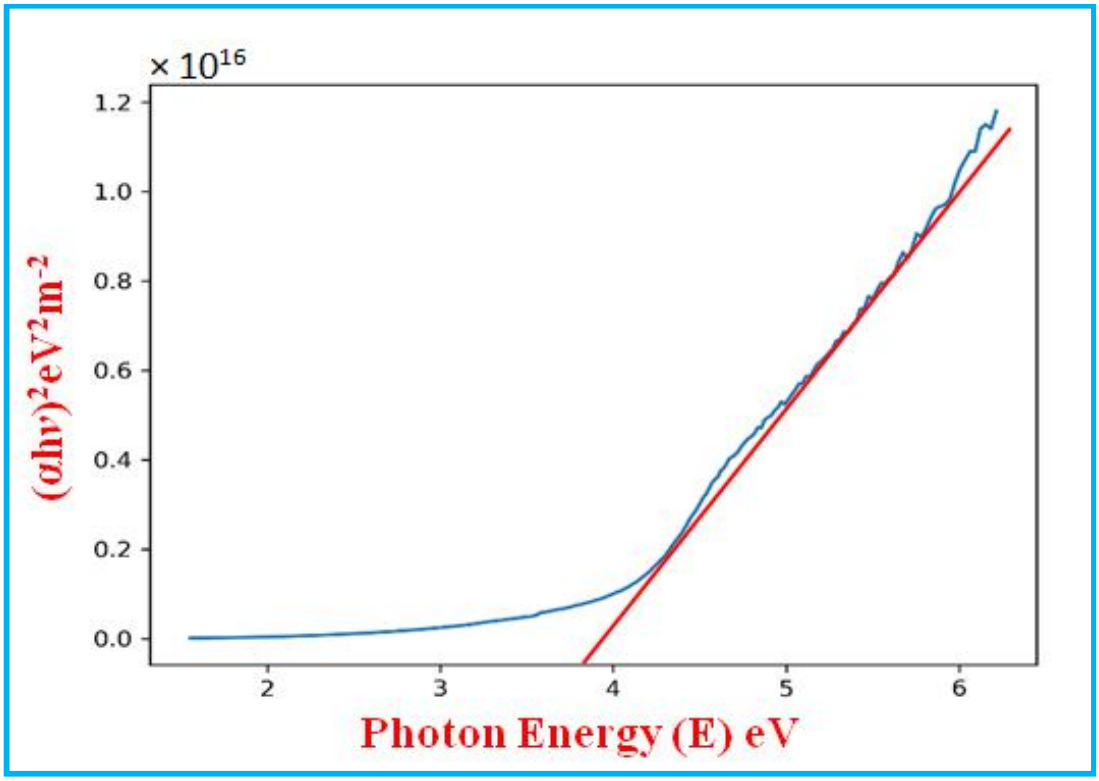

Figure 13: Plot of band energy gap of Rutile.

5.0 Conclusion

In this research, the Rutile nanaoparticle were source and prepared using high energy ball milling technique and characterized for its structural and optical properties. The crystalline size ranged from 52.776nm to 95.529 nm with an average crystalline size of 87.740 nm. Its dislocation density was obtained to be ranged from $(0.109 \times 10^{-3} to\ 0.0359 \times 10^{-3}) nm^{-2}$. The optical properties revealed that Rutile nanoparticles showed relatively high absorbance within the range of 40.9% to 65.8% at the ultraviolet region. However, at the ultraviolet region a constant decrease in the absorbance was observed within 45.4% to 63.6% which further decreased as it approaches the visible region and then decreased to 35.5% at the near infrared region. Furthermore, the transmittance value was observed to be zero at the wavelength of 200 to 300nm which were within the ultraviolet region but increased as it approaches visible region up to 92.8% and increases further to 99.9% in the near-infrared region. The optical conductivity result was seen to be stable as photon energy increases aside the abrupt increase and decrease observed at 2eV of the photon energy. Hence, the band gap of Rutile dispersed in ethanol was obtained to be 3.88eV. This research revealed that Rutile nanoparticle can be prepared using ball milling technique for optoelectronic devices and photovoltaic application such as solar cells.

6.0 Recommendation

Further research should be conducted on determining the magnetic properties and other characteristics of the nanoparticles which can aid in exploring more possible applications of the Rutile particle.

Disclaimer (Artificial intelligence)

Option 1:

Author(s) hereby declare that NO generative AI technologies such as Large Language Models (ChatGPT, COPILOT, etc.) and text-to-image generators have been used during the writing or editing of this manuscript.

Thank you.

Reference

Al-Hammadi A. H., and Sadiq H. K., (2023) Investigations on Optical and Electrical Conductivity of Ba/Ni/Zn/Fe16O27 Ferrite Nanoparticles. Biointerface Research in Applied Chemistry. 13 (2) 168 https://doi.org/10.33263/BRIAC132.168.

Aline L.S., Jeverson T. A., Adalberto F., Gustavo D., (2010). Surface and Quantum Confinement Effects in ZnO Nanocrystals. Journal of Physical Chemistry C 114(43), DOI:10.1021/jp103768v

Ashraf, R., Saira R., Zohra N.K., and Shahzad N., (2015). Structural and magnetic properties of iron doped ZnO nanoparticles. Materials Today: Proceedings 2, 5384 – 5389 doi:10.1016/j.matpr.2015.11.055.

Bromiley, G.D., and Hilairet, N. (2005) Hydrogen and minor element incorporation in synthetic Rutile. Mineralogical magazine 69,345-358.

Carmen, C.P., Susana, F. B., and Wim, M. D.,(2019). Ball milling: a green technology for the preparation and functionalisation of nanocellulose derivatives. Nanoscale Adv., 1, 937. DOI: 10.1039/c8na00238j.

Carruzzo, S., Clarke, D.B., Pelrine, K.M., and MacDonald, M.A. (2006) Texture, composition, and Origin of rutile in the south mountain Batholith, Nova Scotia. Canadian mineralogist 44, 715-729

Chaturvedi, S., and Dave, P.N. (2013) A review on the use of nanometals as catalysts for the thermal decomposition of ammonium perchlorate. J Saudi chem Soc 17(2):135-149.

Choudhary, K.K., Rathore, V., and Dixit, R.C.(2022). Size effect on optical conductivity of Bi_2Te_3Nanoparticles due to softewing of phonon frequencies. Materials Today: proceedings 54: 933-936.

Domtau D.L., Simiyu J., Ayieta E.O., Muthoka B., Mwabora J. M., Optical and Electrical Properties Dependence on Thickness of Screen-Printed TiO_2 Thin Films, Journal of Materials Physics and Chemistry, 2016, Vol. 4, No. 1, 1-3, DOI:10.12691/jmpc-4-1-1

Doyan A.S., Mahardika I.K., Rizaldi D.R., Fatimah Z., (2022) Structure and optical properties of Titanium Dioxide thin film with mixed Fluorine and Indium doping for solar cell components. Journal of Physics: Conference Series, doi:10.1088/1742-6596/2165/1/012009.

Edwin, V.D.P., Frank, A.W.C., Auguste, S., Reink, N., Ton, G.V.L. (2014) Refractive index Determination of nanoparticles in suspension using nanoparticle tracking analysis. ACS Nano letter. 14(11): 6195-6201.

Falak, S.(2010) Crystal structure determination I. Pakistan Institute of Engineering and Applied Sciences.1-41.

Fehmi A., Hikmet E., Fahrettin Y., (2020) Investigation of Optical Properties of TiO_2 Nano Powder. Journal of Natural and Engineering Sciences, DOI: 10.28978/nesciences.756725, 5(2): 68-72

Graham, J., and Morris, R.C. (1973) Tungsten and antimony-substituted rutile. Mineralogical magazine 39,470-473

Gupta, A.K., and Gupta, M. (2005) Synthesis and surface engineering of iron oxide nanoparticles for biomedical applications. Biomaterials, 26(18), 3995-4021.

Hassan, W.F. (1994) Geochemistry and mineralogy of Ta-Nb rutile from peninsular Malaysia. Journal of Southeast Asian Earth Sciences 10,11-23.

Hiroshi, K., Ayumu, I., Katja, O., Ilpo, N.(2016) Refractive index measurement of nanoparticles By immersion refractometry based on a surface plasmon resonance sensor. Chemical Physics letters.654:72-75.

Jothibas, M., Johnson J.S., Manoharan, C., Kartharinal P.I., Praven, P., and Prince R.J.(2017). Structural and optical properties of Zinc Sulphide Nanoparticles synthesized via solid state reaction method. Journal of material science: Materials in Electronics, 28,1889-1894.

Joy, J., Krishnamoorthy, A., Tanna, A., Kamathe, V., Nagar, R., and Srinivasan, S., (2022). Recent Developments on the Synthesis of Nanocomposite Materials via Ball Milling Approach for Energy Storage Applications. Appl. Sci. https://doi.org/10.9734/ajopacs/2024/v12i4234.

Kröhnke C. 2001. Encyclopedia of materials: Science and technology. Elseviers publishers

Liu, X.; Pan, L.; Zhao, Q.; Lv, T.; Zhu, G.; Chen, T.; Lu, T.; Sun, Z.; Sun, C. UV-assisted photocatalytic synthesis of ZnO–reduced graphene oxide composites with enhanced photocatalytic activity in reduction of Cr(VI). Chem. Eng. Journal. 2011, 183, 238–243. doi:10.1016/j.cej.2011.12.068

Madkhali, N. Analysis of Structural, Optical, and Magnetic Properties of (Fe,Co) Co-Doped ZnO Nanoparticles Synthesized under UV Light. Condens. Matter 2022, 7, 63. https://doi.org/10.3390/condmat7040063

Mbonu, J.I.(2015) Determination of Ni(II) crystal structure by powder x-ray diffraction. ScientiaAfricana. 14(1): 158-164.

Murad, E., Cashion, J.D., Noble, C.D., and Pilbrow, J.R. (1995) The chemical state of fe in rutile from an albitite in Norway. Mineralogical Magazine 59,557-560.

Noor, H., Majeed AH, Ahmed H.(2019) Structural, optical and dielectric properties of (PS-In2O3/ZnCoFe2O4) nanocomposites: Egyptian journal of chemistry. Egypt.J.Chem.V 62(2):577-592

Okafor C. E., Okoli N. D., Imosobomeh L. I. (2022) Effect of Doping and Co-sensitization on the Photovoltaic Properties of Natural Dye-sensitized Solar Cells. SSRG International Journal of Applied Physics 9 (3), 44-54, https://doi.org/10.14445/23500301/IJAP-V9I3P105

Onu C.P, Ekpunobi A.J, Okafor C.E, Ozobialu L.A (2023) Optical Properties of Monazite Nanoparticles prepared Via Ball Milling. Asian Journal of Research and Reviews in Physics 7(4): 17 – 29. DOI: 10.9734/AJR2P/2023/v7i4146

Onu C.P, Ekpunobi A.J, Ozobialu L.A, Okafor C.E, Diemiruaye M.J, Muomeliri C.B and Onu C.E (2024) Structural, optical, magnetic and electrical properties of zinc oxide doped with iron: A review. Asian Journal of Physical and Chemical Sciences 12(4): 29 – 40. DOI: 10.9734/AJR2P/2023/v7i4146

Ozobialu, L. A., A. J. Ekpunobi, D. M. Jeroh (2022) Effect of Time on the Optical and Structural Properties of Tin Oxide Thin Films as an Electron Transport Layer for Perovskite Solar Cell. SSRG International Journal of Applied Physics 9 (3), 37-43. https://doi.org/10.14445/23500301/IJAP-V9I3P104

Rice, C., Darke, K., and Still, J (1998) Tungsten-bearing rutile from the Kori Kollo gold mine Bolivia. Mineralogical Magazine 62,421-429.

Rong, P.; Ren, S.; Yu, Q. Fabrications and Applications of ZnO Nanomaterials in Flexible Functional Devices-A Review (2018). Crit. Rev. Anal. Chem.49, 336–349. : https://doi.org/10.1080/10408347.2018.1531691

Saleem, A.H., Rashid, O.K., Sura, N.T.(2016) Structural and optical properties of tin oxide and Indium doped SnO_2 thin films deposited by thermal evaporation technique. Journal of Advances in physics. 12(3): 4394-4399.

Shalini C., Pragnesh N. D., Shah N.K., (2012). Applications of nano-catalyst in new era Journal of Saudi Chemical Society, Volume 16, Issue 3, Pages 307-325, https://doi.org/10.1016/j.jscs.2011.01.015.

Satoshi H, Nick S. Introduction to nanoparticles. Microwave in nanoparticle synthesis, Firsty edition. 2013; 1 – 24.

Scott, K.M. (2005) Rutile geochemistry as a guide to porphyry Cu-Au mineralization, North Parkes, New South Wales, Australia. Geochemistry: Exploration, Environment, Analysis 5,247-253.

Simon K. O., Ekpunobi, A. J., ,Imosobomeh L. Ikhioya (2022) Synthesis and Characterization of ZnS Nanoparticles by Ball Milling Technique. SSRG International Journal of Material Science and Engineering 8 (3), 6-13, https://doi.org/10.14445/23948884/IJMSE-V8I3P102

Smith, D., and Perseil, E.A. (1997) Sb-rich rutile in the manganese concentrations at St. marcel-praborna, Aosta Valley, Italy; Petrology and crystal-chemistry. Mineralogical Magazine 61,65-669.

Srivastava, M., Chaubey, A., and Ojiha, A.K. (2009) Investigation on size dependent structural and magnetic behavior of nickel ferrite nanoparticles prepared by sol-gel and hydrothermal methos. Mater Chem Phys 118(1):174-180

Sta I., Jlassi M., Hajji M., Boujmil M. F., Jerbi R., Kandyla M., Kompitsas M., Ezzaouia H., (2014) Structural and optical properties of TiO_2 thin films prepared by spin coating, J Sol-Gel Sci Technol DOI 10.1007/s10971-014-3452-z

Sutapa, I.W., Abdul W.W., Taba, P., and Nafie N. L., (2018) Dislocation, crystallite size distribution and lattice strain of magnesium oxide nanoparticles. IOP Conf. Series: Journal of Physics: Conf. Series (979)012021 doi :10.1088/1742-6596/979/1/012021.

Tan, X., Jaka, S., Wenrong, Y.,Yongbai, Y., Alexey, M., Glushenkov, Lu, H.L., ,Patrick, C., Howlettb, and Ying, C., (2013) Ball milling: a green mechanochemical approach for synthesis of nitrogen doped carbon nanoparticles. Nanoscale, 5, 7970. DOI: 10.1039/c3nr02328a.

Wang, Y., Sun, C., Zhao, X., Cui, B., Zeng, Z., Wang, A., Lui, G., and Cui, H. (2016) The application of Nano-TiO_2 photo semiconductors in Agriculture Nanoscale Res. Lett 11:529-535.

Wanjala, K. S., Njoroge, W. K., and Ngaruiya, J. M. (2016). Optical and electrical characterization of ZnS: Sn thin films for solar cell application. Int. J. Energy Enginneering, 6(1).

Yetter, A.R., Risha, G.A., and Son, S.A. (2009) Metal particle combustion and nanotechnology. P Combust Inst. 32(2):1819-1838.

Zack, T., Kronic, A., Foley, S.F., and Rivers, T. (2002) Trace element abundances in rutile from eclogites and associated garnet mica schists. Chemical Geology 184,97-122.

Zhang, J., Zhou, P., Lui, J., and Yu, J. (2014) New understanding of the difference of photocatalytic activity among anatase, rutile and brookite TiO_2. Phys. Chem. Phys. 16,20382-20386.